Transport Dynamics and Multi-Scale Coupling of Turbulence

S. Inagaki[1)], N. Tamura[2)], Y. Nagashima[1)], T. Tokuzawaa[2)], T. Yamada[1)], K. Ida[2)], T. Maruta[3)], S. Kubo[2)], K. Terasaka[3)], T. Shimozuma[2)], Y. Nagayama[2)], K. Kawahata[2)], A. Komori[2)], S. Shinohara[3)], A. Fujisawa[2)], M. Yagi[1)], Y. Kawai[1)], S.-I. Itoh[1)], K. Itoh[2)] and the LHD experimental group

[1)]*RIAM, Kyushu University, 6-1 Kasuga-Koen, Kasuga 816-8580, Japan*
[2)]*National Institute for Fusion Science,322-6 Oroshi-cho, Toki 509-5292, Japan*
[3)]*IGSES, Kyushu University, 6-1 Kasuga-Koen, Kasuga 816-8580, Japan*

Correlation between electron heat flux and electron temperature gradient is obtained in cold pulse experiments. Evidence for a long distance correlation is found in plasma, where the nonlocal temperature rise is observed. Multi-scale coupling of density fluctuation is analysed by using envelope method. Existence of the low frequency ($\leq$ 2 kHz) modulator of the density fluctuation is suggested in a nonlocal plasma.

Keywords: dynamics, nonlocal, correlation, fluctuation, LHD

1 Introduction

Turbulence transport is higher than the neoclassical level in the edge to intermediate region in helical devices (heliotron, stellarators, heliac and others) as well as in tokamaks. The turbulence causes not only quantitative features of transport but also qualitative ones. Transport dynamics reveals such qualitative features of transport. Various transient transport phenomena observed in helical plasmas indicate complexities of turbulent transport. Recent theoretical works on drift wave turbulence show drift waves are strongly coupled with micro-scale, meso-scale and macro-scale waves. These non-linear couplings form turbulent structures, which have strong influences on transport. Thus, the dynamics and the multi-scale coupling of drift waves are now the most important issues to be clarified in transport studies. A comprehensive understanding of transport dynamics through first principle turbulence models is strongly required for achieving predictive capability of turbulence transport.

2 Nonlocal Transport in LHD

Some local transport models based on temperature-gradient-driven turbulence indicate that the heat transport is non-linear and thus the electron heat diffusivity, χ_e, has a dependence on electron temperature, T_e, and/or electron temperate gradient, ∇T_e [1]. To study the non-linearity of heat transport, transient transport analysis is recognized as a very powerful tool because it can yield $\partial q_e/\partial \nabla T_e$ and $\partial q_e/\partial T_e$, here q_e is the electron heat flux [2]. The transient experiments (inducing cold and/or heat pulses) have been performed and many non-linear transport models have been proposed and tested[3]. However, fast propagation of a temperature perturbation were observed, for example, the ballistic propagation observed in TJ-II[4], the heat pulse propagation caused by L-H transition [5] and heating power switching [6]. If χ_e has a dependence like $\chi_e \propto \nabla {T_e}^{\alpha}$, $\alpha \sim 50$ is required to explain these transient responses. Fast cold pulse propagation is also observed in the Large Helical Device (LHD) [7]. Figure 1 shows typical time evolution of a cold pulse induced by a tracer encapsulated solid pellet (TESPEL) injection in the low density (1×10^{19}m^{-3}) NBI plasma on LHD (a major radius at the magnetic axis of R_{ax} = 3.5/3.6 m, an averaged minor radius of a = 0.6 m and a magnetic field at axis of up to 2.83T) [8]. The simulation results based on models of $\chi = \chi_{pb}$ and $\chi_e \propto \nabla {T_e}^{\alpha}$ are also shown, here χ_{pb} is a heat diffusivity determined from the power balance analysis in

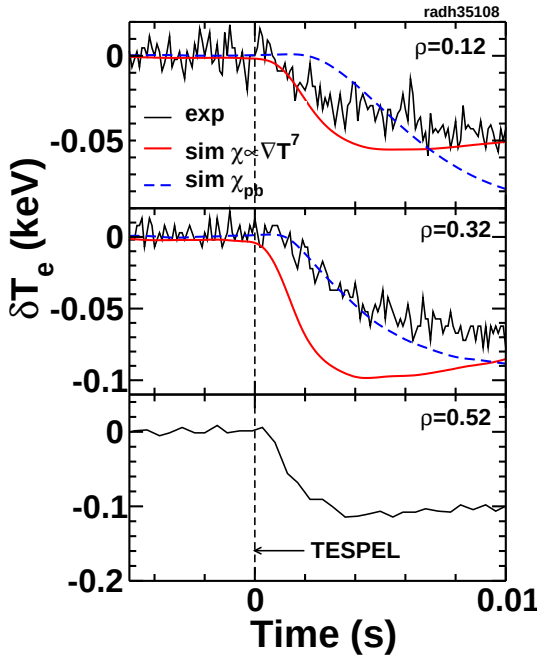

Fig. 1 Time evolution of δT_e at three different normalized radii. The simulation results based on models of $\chi = \chi_{pb}$ and $\chi_e \propto \nabla {T_e}^{\alpha}, \alpha = 7$ are also shown.

author's e-mail: inagaki@riam.kyushu-u.ac.jp

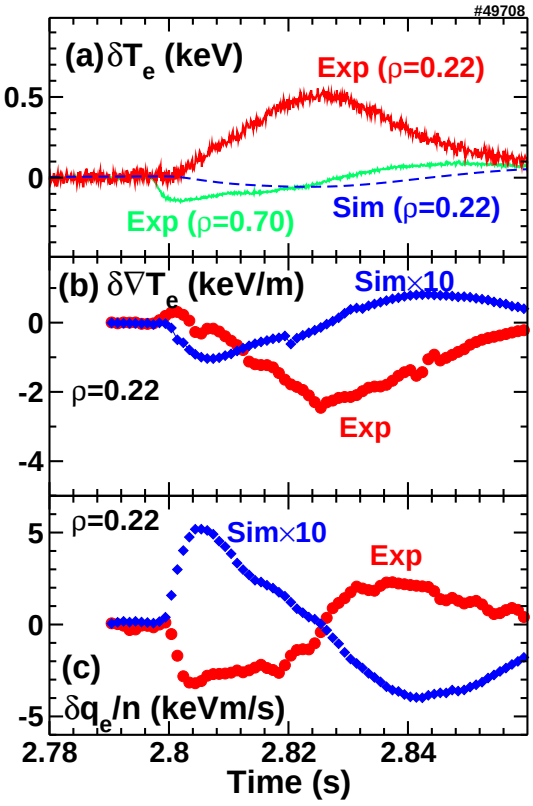

Fig. 2 Time evolution of (a) δT_e at two different normalized radii, (b) $\delta\nabla T_e$ at $\rho = 0.22$ and (c) δq_e at $\rho = 0.22$. Simulation result based on the power balance χ model are also shown. Simulated results are much smaller than experimental observations, and thus, simulation results are multiplied by ten in this figure.

stationary state [9]. In simulation, the electron temperature perturbation, δT_e, is calculated from the perturbation equation written as

$$\frac{3}{2}n_e\frac{\partial\delta T_e}{\partial t} = -\nabla\cdot\delta q_e. \tag{1}$$

The core T_e begins to decrease before the diffusive transport effect (calculated by χ_{pb}) reaches this region. To explain this prompt response of the core T_e by the nonlinearity of χ_e, a strong ∇T_e dependence of χ_e ($\alpha = 7$) is required. On the other hand, $\alpha = 1 - 3/2$ is required to explain the stationary transport property both in tokamaks and helical devices [9]. A new perspective to turbulence transport (i.e. non-locality) has been introduced to explain this discrepancy.

In addition, the response to edge cold pulses often have reversed polarity, with the core T_e increasing in response to edge cooling in many tokamaks and LHD [10, 11, 12, 13, 14]. A significant core T_e rise has been observed by TESPEL injection in LHD as shown in Fig. 2 (for more details see [13]). Typical parameters in this experiment are as following: line averaged density $1 - 2 \times 10^{19}\mathrm{m}^{-3}$, central electron temperature up to 1.5 keV, central ion temperature of 1-2 keV, plasma β value of 0.1%, absorbed ECH power of 0.8 MW, deposited neutral beam power of 2 MW. Characteristic time and spacial scales are ion Larmor radius $\rho_i \sim 1$ mm, $c/\omega_p \sim 2$ mm, typical spatial scale of meso-scale structure $\sqrt{a\rho_i} \sim 30$ mm, $a/c_s \sim 1\mu s$, global energy confinement time of 50 ms, meso-scale time $\sqrt{(a/\rho_i)(a/c_s)} \sim 30\mu s$, where ω_p is the plasma frequency, c is the speed of light and c_s is the ion sound velocity. The relationship between heat flux and temperature gradient is essential to understand heat transport. Thus, time evolutions of the core ∇T_e perturbation and the heat flux perturbation (normalized by density) are also shown in Fig. 2. Multi-channel heterodyne radiometer is used to track the small T_e perturbations at different normalized radii [15]. The absolute error of ∇T_e determined by the absolute calibration of ECE is 20% and the relative errors of the ∇T_e determined by the noise levels of ECE is only 1%. The electron heat flux perturbation can be determined from the perturbation equation written as and it can be written as,

$$\delta q_e(\rho,t) = -\frac{1}{S(\rho)}\int_0^\rho \frac{3}{2}n_e\frac{\partial\delta T_e(\rho,t)}{\partial t}dV, \tag{2}$$

where S is the surface area of the closed flux surface, V is the volume. The power balance simulation indicates small changes in the temperature gradient and heat flux in the core region and they are quite different from experimental observations. In addition, the local transport assumption can not explain the sign of change in the heat flux. In spite of the smooth change in the temperature gradient, abrupt reductions in the heat flux (heat flux jump) are observed after several ms from the TESPEL injection.

To determine the nonlocal correlation between the heat flux and the temperature gradient, two-point cross-correlations between the core and the edge are calculated. The cross-correlation is defined as $C_{f,g}(\rho_{ref},\rho,\tau) = \langle f(\rho_{ref},t)g(\rho,t+\tau)\rangle / \sqrt{\langle f^2(\rho_{ref},t)\rangle\langle g^2(\rho,t)\rangle}$, here $\langle\rangle$ means temporal average, defined as $\langle h(t)\rangle = (T)^{-1}\int_0^T h(t)dt$. Figure 3 indicates time evolution of cross correlations, $C_{\delta q_e/n_e,-\delta\nabla T_e}(\rho_{\delta q_e/n_e},\rho_{\delta\nabla T_e},\tau)$, between core to core (local: $\rho_{\delta q_e/n_e} = 0.19$, $\rho_{\delta\nabla T_e} = 0.19$), core to edge (non-local: $\rho_{\delta q_e/n_e} = 0.19$, $\rho_{\delta\nabla T_e} = 0.58$), edge to core (non-local: $\rho_{\delta q_e/n_e} = 0.58$, $\rho_{\delta\nabla T_e} = 0.19$) and edge to edge (local: $\rho_{\delta q_e/n_e} = 0.58$, $\rho_{\delta\nabla T_e} = 0.58$). In the paradigm for local transport, a strong correlation between $q_e(\rho)$ and $\nabla T_e(\rho)$ is trivial and the relation of $\delta q_e = -n_e\chi_{pb}\nabla\delta T_e$ is indeed satisfied in a simulation. On the other hand, experimental result indicates that core ($\rho = 0.19$) heat flux is strongly coupled with edge ($\rho = 0.58$) temperature gradient for a short time lag, and therefore, a presence of the long distance/non-local correlation between heat flux and temperature gradient is clarified. The strong negative non-local correlation is reduced with a increase in the time lag. The correlation time, which is defined as peak width of time lag at half height, is 8 ms. This time is much longer than a/c_s and $\sqrt{(a/\rho_i)(a/c_s)}$. The local core to core correlation indicates a gradual reduction similar to that predicted by local transport when $\tau \geq 15$ ms. Subsequently, the non-local correlation is dominant over the local correlation. The edge

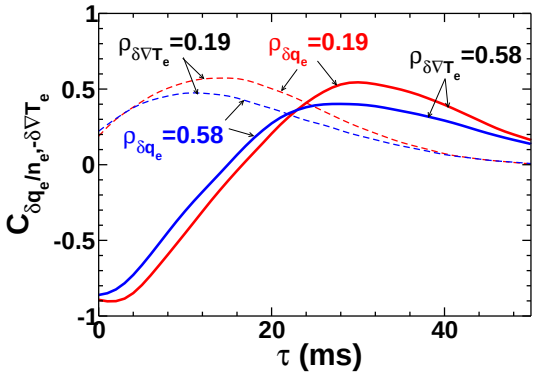

Fig. 3 Time evolution of cross correlations between core to core ($\rho_{\delta q_e/n_e} = 0.19$, $\rho_{\delta\nabla T_e} = 0.19$), core to edge ($\rho_{\delta q_e/n_e} = 0.19$, $\rho_{\delta\nabla T_e} = 0.58$), edge to core ($\rho_{\delta q_e/n_e} = 0.58$, $\rho_{\delta\nabla T_e} = 0.19$) and edge to edge ($\rho_{\delta q_e/n_e} = 0.58$, $\rho_{\delta\nabla T_e} = 0.58$).

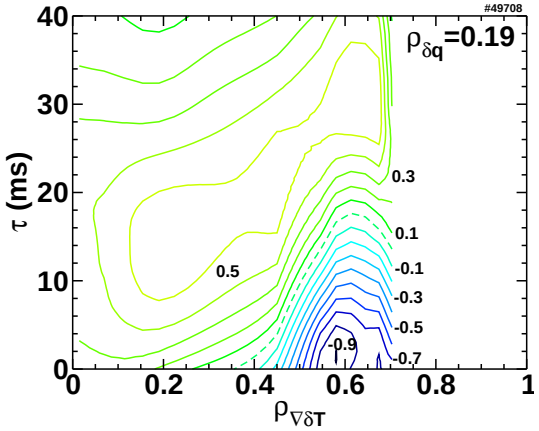

Fig. 4 Contour map of cross correlation between δq_e at $\rho = 0.19$ and $\delta\nabla T_e$ at different normalized radii.

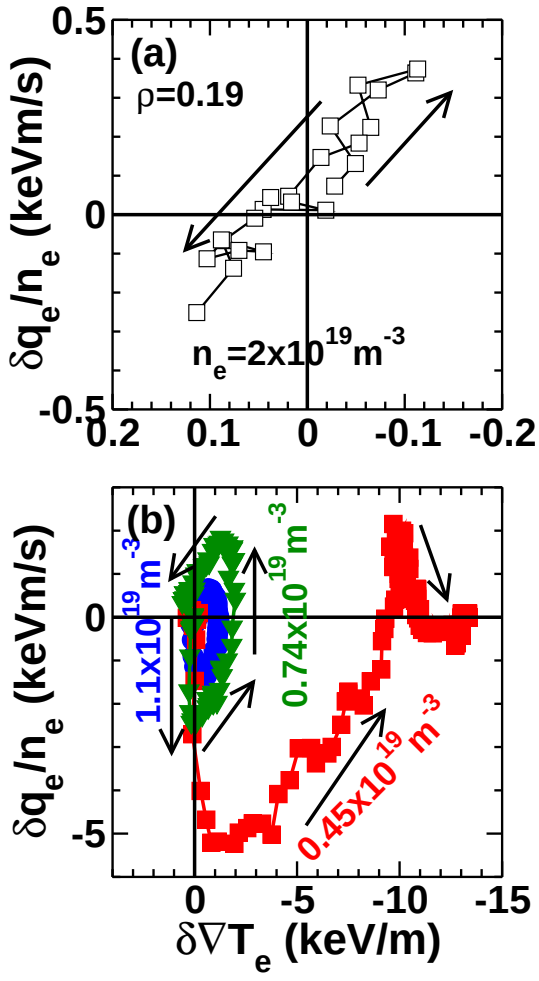

Fig. 5 Flux-gradient Lissajous diagrams at $\rho = 0.19$ in (a) the local transport condition (density is above critical value) and (b) the nonlocal condition (density is below critical value). The arrows denote the direction of variation.

heat flux is not coupled with core temperature gradient. The local edge to edge correlation indicates strong negative coupling, i.e. a decrease in the flux with an increase in the gradient (negative heat diffusivity). The negative heat diffusivity is often observed in the transition phase. Some sort of transition, thus, may take place in the nonlocal T_e rise phenomena.

To demonstrate a presence of the long distance correlation in turbulent transport, the cross correlations between the core heat flux and the temperature gradient at different normalized radii is shown in fig. 4. This diagram indicates the temperature gradient at $\rho = 0.54-0.61$ has strong negative correlation (≤ -0.8) with the core heat flux. The obtained correlation length ($0.6a$) is obviously larger than the so-called meso-scales and thus the global scales. A presence of the long distance/nonlocal correlation between heat flux and temperature gradient is clarified.

The nonlocal T_e rise takes place in the low-n_e and high-T_e (low collisionality) regime in LHD just as TFTR scaling predicts.[13, 14, 11]. The critical density for nonlocal T_e rise is $1.5 \times 10^{19}\mathrm{m}^{-3}$ in LHD. This value is 2-3 times larger than that for eITB formation ($0.6 \times 10^{19}\mathrm{m}^{-3}$).

The relations between the heat flux and the temperature gradient are determined both above and below the critical condition and shown in fig. 5. The heat transport above the critical condition is considered to be dominated by local processes. As shown in Fig. 5(a), the obtained data lie on the straight line. In other words, local heat flux is proportional to local temperature gradient. On the other hand, Lissajous diagrams (Fig. 5(b)) reveal hysteresis in heat flux versus temperature gradient. After the TESPEL injection, the heat flux changes abruptly and discontinuously. This flux jump is not accompanied by a change in the local temperature gradient, therefore transport is non-diffusive and non-local. The area of the hysteresis loop increases with a decrease in the density. The density is close to the critical value for the eITB formation, the nonlocal T_e rise triggers the eITB formation.

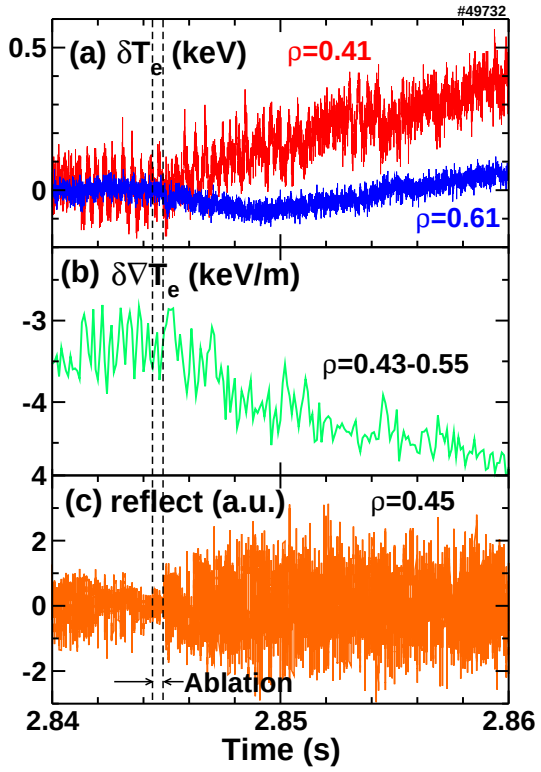

Fig. 6 Time evolution of (a) δT_e at $\rho = 0.41$ and 0.61, (b) averaged temperature gradient in the region of $\rho = 0.43-0.55$ and (c) X-mode reflectmetry signal at $\rho = 0.45$.

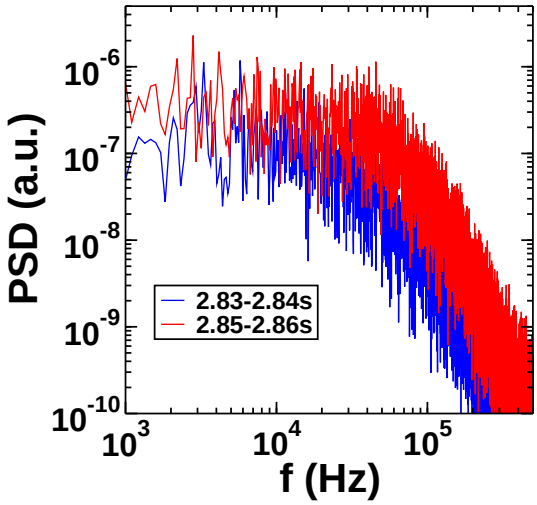

Fig. 7 Change of power spectral density of reflectmetry signal at $\rho = 0.45$. Note the high pass filter ($\geq$ 1 kHz) is applied to the reflectmetry signal.

3 Envelope Analysis

The nonlocal mechanism in plasma considered to be implicated in a structure, which is generated by interactions of turbulence over long distances. Models assuming the existence of the fluctuations with long radial correlation length on the order of the minor radius has successfully explained several features of nonlocal transport dynamics [16]. However, the experimental observation for the structures with a long correlation length has not been observed. For further study of nonlocal transport, experimental observations of spatiotemporal structure of turbulence is essential. Langmuir probe diagnostics are most suitable to fulfill a high temporal and spatial resolution measurement of fluctuations. The low temperature plasma, therefore, is very useful to study structures in turbulent plasma. The drift wave turbulence is successfully excited in the LMD-U plasmas [17]. The LMD-U has a linear magnetic configuration. In other words, geometrical effects due to configuration can be simplified. Thus, thermodynamical and statistical features of plasma turbulence will be emphasized in the turbulent structure formation. Thereby, results obtained in LMD-U experiments have a commonality beyond configuration differences. The many analysis tools are developed and tested in LMD-U. The non-linear coupling of fluctuation is identified by using bi-spectral analysis. Envelope analysis is also one of new tools.

In toroidal plasmas, the most common methods to measure fluctuations are those for density fluctuations such as conventional reflectometry. However, it is difficult to detect a certain type of fluctuation (e.g. zonal flows) by simply using the density fluctuation diagnostics due to the low level of density fluctuation component. Recent progress in the fluctuation diagnostics (e.g. HIBP[18]) has clarified non-linear coupling of drift wave turbulence and structures. For example, the turbulent density fluctuations are modulated by the zonal flows through the parametric modulational instability[19]. Thus, density fluctuations have some information about structures which can modulate them [20]. The multi-channel reflectmetry, thereby, has a capability to measure a correlation length of structure. Two channel X-mode reflectmetry was worked on the low density plasma in LHD. Figure 6 shows typical time evolution of a refrectmetry signal during the nonlocal T_e rise. After a TESPEL injection, T_e at $\rho = 0.61$ drops and T_e at $\rho = 0.41$ rises, hence, temperature gradient begins to increase. The refrectmetry signal ($\geq$ 10kHz) at $\rho = 0.45$ increases after TESPEL injection as shown in Fig. 7. This enhancement of density fluctuation may be driven by an increase in pressure gradient at $\rho = 0.45$. In order to deduce the existence of modulator, the envelope analysis is applied. Figure 8 shows an example of signal envelope and power spectrum densities of the envelope. An envelope is calculated from a high-pass filtered signal ($\leq$100kHz) by using of Hilbert transform. The refrectmetry signal data in stationary state before TESPEL injection are used to make ensemble averaging for reduction of statistical error. It is found that the envelope is modulated. The power spectrum density at $\rho = 0.45$ appears an existence of the modulator in the low frequency region ($\leq$2kHz). The geodesic acoustic mode (GAM) frequency is higher (~10kHz) than that of the modulator, and thus GAM is ruled out as a candidate of the modulator. There is no significant MHD mode

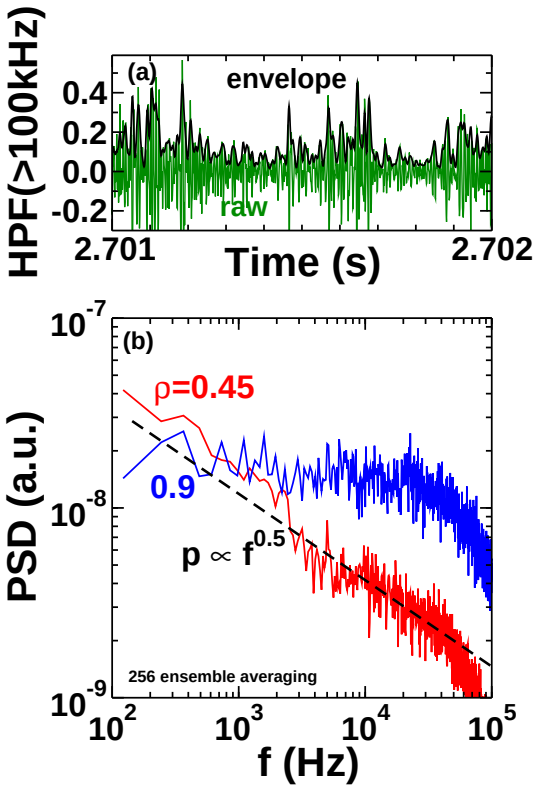

Fig. 8 (a) Time evolution of high-pass filtered signal (≤100kHz) at $\rho = 0.45$ and its envelope, (b) Power spectrum density of envelopes at two different normalized radii.

observed with the magnetic measurement system. In theoretical works, fluctuation of the long wave length mode excited from background micro fluctuation is predicted as the candidate[21]. On the other hand, there is no clear modulator in the power spectrum density at $\rho = 0.9$ and no strong coherence between envelopes at $\rho = 0.45$ and $\rho = 0.9$. The core heat flux is correlated to the edge temperature gradient around $\rho = 0.6$, thus, reflectmetry around $\rho = 0.6$ is required to discuss the correlation length of a observed modulator. The multi-channel reflectmetry and coherence and bi-spectral analysis will be the object of future work.

4 Summary

In summary, we investigate the dynamical structure of LHD cold pulse experiments providing experimental evidence for the presence of nonlocal coupling. We have found that 1) a correlation structure which have, indeed, the global spatiotemporal scales exists in turbulent plasma, 2) existence of turbulent density fluctuation modulators with low frequency.

Acknowledgments

We thank Professor O. Motojima for his continuous encouragements. We are grateful to the technical group for their excellent support. This work is partly supported by a grant-in-aid for Specially-Promoted research (16002005) and by the collaboration programs of NIFS (NIFS07KOAP017).

References

[1] F. Ryter *et al* , Phys. Rev. Lett. **86** (2001) 5498
[2] N. J. Lopes Cardozo, Plasma Phys. Control. Fusion **37** (1995) 799
[3] S. Inagaki *et al* , Nucl. Fusion **46** (2006) 133
[4] B. P. van Milligen *et al* , Nucl. Fusion **42** (2002) 787
[5] V. V. Parail *et al* , Nucl. Fusion **37** (1997) 481
[6] U. Stroth *et al* , Plasma Phys. Control. Fusion **38** (1996) 1087
[7] O. Motojima *et al* , Nucl. Fusion **43** (2003) 1674
[8] S. Sudo *et al* , Plasma Phys. Control. Fusion **44** (2002) 129
[9] H. Yamada *et al* , Nucl. Fusion **43** (2003) 749
[10] K. W. Gentle *et al* , Phys. Rev. Lett. **74** (1995) 3620
[11] M. W. Kissick *et al* , Nucl. Fusion **38** (1998) 821
[12] P. Mantica *et al* , Phys. Rev. Lett. **82** (1999) 5048
[13] S. Inagaki *et al* , Plasma Phys. Control. Fusion **48** (2006) A251
[14] N. Tamura *et al* , Nucl. Fusion **47** (2007) 449
[15] K. Kawahata *et al* , Rev. Sci. Instrum. **74** (2003) 1449
[16] T. Iwasaki *et al* , J. Phys. Soc. Japan **68** (1999) 478
[17] K. Terasaka *et al* , Plasma Fusion Res. **2** (2007) 031
[18] A. Fujisawa *et al* , Phys. Rev. Lett. **93** (2004) 165002
[19] K. Itoh P. H. Diamond, S.-I. Itoh and T. S. Hahm, Plasma Phys. Control. Fusion **47** (2005) R5
[20] Y. Nagashima *et al* , Plasma Phys. Control. Fusion **49** (2007) 1611
[21] S.-I. Itoh and K. Itoh, Plasma Phys. Control. Fusion **43** (2001) 1055